Genetic and functional implications of an exonic *TRIM55* variant in heart failure

Juho Heliste, MD[a,b,c]; Himanshu Chheda, MSc[a]; Ilkka Paatero, PhD[d]; Tiina A. Salminen, PhD[e]; Yevhen Akimov, MSc[a]; Jere Paavola, MD, PhD[f]; Klaus Elenius, MD, PhD[b,d,g,h] and Tero Aittokallio, PhD[a,i,*]

[a]Institute for Molecular Medicine Finland, FIMM, University of Helsinki, Biomedicum 2U, Tukholmankatu 8, FI-00290 Helsinki, Finland

[b]Institute of Biomedicine, University of Turku, Kiinamyllynkatu 10, FI-20014 Turku, Finland

[c]Turku Doctoral Programme of Molecular Medicine, University of Turku, Turku, Finland

[d]Turku Bioscience Centre, University of Turku and Åbo Akademi University, Tykistökatu 6, FI-20520 Turku, Finland

[e]Structural Bioinformatics Laboratory, Biochemistry, Faculty of Science and Engineering, Åbo Akademi University, Tykistökatu 6, FI-20520 Turku, Finland

[f]Unit of Cardiovascular Research, Minerva Foundation Institute for Medical Research, Biomedicum 2U, Tukholmankatu 8, FI-00290 Helsinki, Finland

[g]Medicity Research Laboratories, University of Turku, Tykistökatu 6, FI-20520 Turku, Finland

[h]Department of Oncology, Turku University Hospital, PO Box 52, FI-20521 Turku, Finland

[i]Department of Mathematics and Statistics, University of Turku, Vesilinnantie 5, FI-20014 Turku, Finland

* Corresponding author:
Tero Aittokallio, PhD, Professor
Institute for Molecular Medicine Finland, University of Helsinki
Biomedicum 2U, Tukholmankatu 8, FI-00290 Helsinki, Finland
tel. +358-503182426; fax: +358 2941 25737; email: tero.aittokallio@fimm.fi

Word count: 6136

Abstract

Background: To tackle the missing heritability of sporadic heart failure, we screened for novel heart failure-associated genetic variants in the Finnish population and functionally characterized a novel variant *in vitro* and *in vivo*.

Methods and results: Heart failure-associated variants were screened in genotyping array data of the FINRISK study, consisting of 994 cases and 20,118 controls. Based on logistic regression analysis, a potentially damaging variant in *TRIM55* (rs138811034), encoding an E140K variant, was selected for validations. In HL-1 cardiomyocytes, we used CRISPR/Cas9 technology to introduce the variant in the endogenous locus, and additionally TRIM55 wildtype or E140K was overexpressed from plasmid. Functional responses were profiled using whole-genome RNA sequencing, RT-PCR and Western analyses, cell viability and cell cycle assays and cell surface area measurements. In zebrafish embryos, cardiac contractility was measured using videomicroscopy after CRISPR-mediated knockout of *trim55a* or plasmid overexpression of TRIM55 WT or E140K. Genes related to muscle contraction and cardiac stress were highly regulated in *Trim55* E140K/- cardiomyocytes. When compared to the WT/WT cells, the variant cells demonstrated reduced viability, significant hypertrophic response to isoproterenol, p21 protein overexpression and impaired cell cycle progression. In zebrafish embryos, the deletion of *trim55a* or overexpression of TRIM55 E140K reduced cardiac contractility as compared to embryos with wildtype genotype or overexpression of WT TRIM55, respectively.

Conclusions: A previously uncharacterized TRIM55 E140K variant demonstrated a number of functional implications for cardiomyocyte functions *in vitro* and *in vivo.* These findings suggest a novel role for *TRIM55* polymorphism in predisposing to heart failure.

Keywords: CRISPR/Cas9; genetic variation; heart failure; TRIM55; rs138811034

1. Introduction

Heart failure is a lethal cardiac disorder with various causes. The overall prevalence of heart failure is 1-2% in a general population [1], while the lifetime risk for people at age of 55 has been estimated to be 33% for men and 29% for women [2]. Genetic background of heart failure risk is only partly understood. In total, approximately 18% of heart failure risk is explained by heritable factors [3]. However, no common genes or signaling pathways accounting for majority of the heritability of heart failure are currently known [4]. Functional characterization of novel heart failure-associated genetic variants would therefore help in identifying key proteins and pathways underlying the pathogenesis. Population-specific genetic risk factors enable genetic screenings and more thorough clinical follow-up as well as early treatment of the high-risk individuals. Genetic findings may also lead to the discovery of novel therapeutic targets for heart failure.

Several genetic variants causing familial cardiomyopathies and related heart failure are well characterized. A large proportion, up to 50%, of the hypertrophic cardiomyopathy syndromes are caused by mutations in *MYBPC3* and *MYH7* genes [5]. For dilated cardiomyopathy, the genetic background is well-defined in approximately 30-35% of the cases where *TTN*, *LMNA*, *MYH7* and *TNNT2* account for the majority of the cases [5]. For sporadic heart failure, the landscape of contributing genes is wider and the results of individual variants are often controversial [6]. For instance, variants in genes related to renin-angiotensin-aldosterone system (*ACE*, *AT1R*, *AGT*), sympathetic nervous system (*ADRB1*, *ADRB2*, *ADRA2C*), inflammatory system (e.g. *CTLA4*, *IL4*) and drug metabolism (*CYP2D6*) have been identified as modifiers of susceptibility, therapeutic response and prognosis of heart failure [6].

TRIM55 gene encodes a protein known as TRIM55 or MURF2, which is highly expressed in the heart and skeletal muscle. TRIM55 contains a RING zinc finger domain and it has been shown to be involved in muscle sarcomere assembly and to function as a ubiquitin E3

ligase [7]. Loss of its function, together with *Trim63*, causes heart failure and cardiac hypertrophy in newborn mice, their functions being thus necessary but redundant [8]. In another study on a knockout mouse model, loss of both *Trim55* and *Trim63* caused severe cardiac hypertrophy, while the loss of each gene alone caused only mild, statistically non-significant increase in heart weight [9]. In a model of experimental hypertrophy using transaortic constriction, hypertrophic response was significantly more pronounced in mice lacking *Trim63*, while mice lacking *Trim55* did not demonstrate any difference to wildtype controls [10]. However, in a mouse model of diabetic cardiomyopathy, *Trim55* knockout mice developed more severe hypertrophy and early onset systolic dysfunction [11]. Additionally, in a rat model of spontaneous cardiac hypertrophy, *Trim55* expression was negatively correlated with left ventricular mass, and in human samples, *TRIM55* expression was lower in idiopathic dilated cardiomyopathy, as compared to healthy heart [12]. *TRIM55* is thus implicated in heart failure pathogenesis but the effects of any deleterious genetic variants have not been characterized in detail earlier.

Here, we carried out a genetic screening for novel variants associated with heart failure using genotyping array and outcome data from a large, Finnish population-based FINRISK survey study [13]. Based on the genetic screening results, a potentially damaging exonic variant in *TRIM55*, encoding E140K variant in the protein, was selected for further validation *in vitro* and *in vivo*. The variant was shown to affect cardiomyocyte-specific functions in CRISPR/Cas9-modified HL-1 cardiomyocytes and contractility of the zebrafish heart. These findings suggest a novel role for a previously uncharacterized TRIM55 E140K variant, where the effect of the variant may be even dominantly negative on heart failure pathogenesis.

2. Materials and Methods

Detailed methods are available in the data supplement. Briefly, CRISPR/Cas9 technology was used to introduce the TRIM55 E140K variant, identified in GWAS analysis for heart failure in the FINRISK data, in the endogenous locus in HL-1 cardiomyocytes. Additionally, plasmid overexpression of TRIM55 wildtype and E140K variant was used in functional analyses. Transcriptional and protein-level responses were profiled using whole-genome RNA sequencing, RT-PCR and Western analyses, respectively. Cellular responses were measured using cell viability and cell cycle assays, immunofluorescence microscopy and cell surface area measurements. In zebrafish embryos, cardiac contractility was measured using videomicroscopy after CRISPR-mediated knockout of *trim55a* or plasmid overexpression of TRIM55 WT or E140K. Zebrafish experiments were conducted according to normal procedures and regulations under the license no. MMM/465/712-93 (issued by the Finnish Ministry of Forestry and Agriculture). The genetic and clinical data from the FINRISK study cohort [13] are available from the THL Biobank of the National Institute for Health and Welfare upon research application.

3. Results

3.1 A previously uncharacterized exonic variant in TRIM55 is associated with heart failure in the Finns

Heart failure-associated genetic variants were screened for in the Finnish population using the genotyping array and outcome data from the FINRISK study. Forty-seven percent (698 individuals) of the individuals with heart failure in the cohort had coronary artery disease. Imputed genotype data passing quality control were available for 20,118 individuals, out of which 994 had heart failure. Logistic regression analysis confirmed several loci previously associated with heart failure that demonstrated nominal association in the Finnish population cohort ($P < 0.001$), either with heart failure or cardiomyopathies, including *ACE* [6], *ANKRD1*,

DSG2, *MYBPC3* and *TTN* [5]. There were four genome wide-significant variants ($P < 5 \times 10^{-8}$), all located in chromosome 16 (Table 1).

The regions with most highly-associated variants were examined in detail to identify candidate causal coding variants in linkage disequilibrium (LD) with the lead variants (LocusZoom plots of selected regions are shown in Supplemental Figure S1). To make the functional validations feasible in the cardiomyocytes, we narrowed our analyses to exonic, coding variants only. Of the most significantly heart failure-associated variants (Table 1), the lead single nucleotide polymorphism (SNP) rs143488191 in chromosome 16 in intergenic region between *RRN3P2* and *SNX29P2* did not have any common coding variants in high LD. A coding variant in *SPN* gene, rs2229654, was strongly associated with heart failure, but *SPN* is mostly expressed in leukocytes, making it less attractive for functional validations. Similarly, the variant in chromosome 12, rs73407741, is intronic and the *FAM222A* gene is predominantly expressed in neural and endocrine tissues.

The lead variant in the chromosome 8, rs117667921, is located in an intron of *ADHFE1*, which encodes the iron containing alcohol dehydrogenase 1 (Fig. 1A). An exonic variant rs138811034 in *TRIM55* gene was found to be in complete LD with the lead SNP (D' = 1). Rs138811034 did not demonstrate an independent association with heart failure in our study cohort (OR 1.522, $P = 0.377$) (Table 2), probably due to lack of resolution in the genotyping array. Minor allele frequency for the variant in the Finnish population is 0.16%, and in other, non-Finnish European populations it is 0.23%, based on the gnomAD database [14]. The variant encodes a missense E140K variant in the TRIM55 protein that is potentially damaging as predicted with the Ensembl Variant Effect Predictor [15]. *TRIM55* has previously been shown to have implications on development of the heart in mouse models [7]. Additionally, loss of TRIM55 is associated with hypertrophy and heart failure in mouse and rat models [11,12] and

in human [12,16]. However, the E140K variant has not been studied earlier in detail, and it was therefore selected for further functional validation.

Table 1. Ten most significant heart-failure associated variants in the FINRISK cohort.

Chromosome	rsID or position	Alternative allele	OR	*P*-value	Gene
16	chr16:29134700	A	3.776	4.07×10^{-9}	
16	chr16:29257381	A	3.280	1.87×10^{-8}	
16	rs143488191	T	3.333	2.09×10^{-8}	
16	rs148456921	A	3.311	4.08×10^{-8}	
16	chr16:29371099	A	3.282	5.07×10^{-8}	
16	rs199707538	G	3.255	6.05×10^{-8}	
16	rs2229654	G	3.274	8.65×10^{-8}	*SPN*
12	rs73407741	T	0.5688	1.64×10^{-7}	*FAM222A*
8	rs117667921	A	2.366	2.45×10^{-7}	*ADHFE1*
4	rs77080662	T	2.400	2.64×10^{-7}	

OR, odds ratio

Table 2. The lead variant in chromosome 8 and two variants in high LD with the lead variant.

Chromosome	rsID	Alternative allele	OR	P-value	Gene	MAF
8	rs117667921	A	2.366	2.45×10^{-7}	*ADHFE1*	0.017
8	rs138811034	A	1.522	0.377	*TRIM55*	0.0016
8	rs112144279	A	2.124	4.46×10^{-6}	*DNAJC5B*	0.017

MAF, minor allele frequency (in the Finnish population based on gnomAD database); OR, odds ratio

3.2 3D model for TRIM55 reveals a surface exposed location for the E140K variant

To predict the position and putative consequences caused by the E140K variation on the 3D structure and molecular interactions of TRIM55, dimeric 3D models for the TRIM55 B2 domain were constructed by homology modeling based on the X-ray structure of TRIM63. Despite the slightly higher sequence identity between TRIM54 and TRIM55, TRIM63 structure was selected as a template (Supplemental Figure S2A) since its two different dimeric forms have been evaluated in detail by Mrosek et al. [17]. Based on their analysis, the dimeric form in the asymmetric unit of the crystal, which corresponds to the dimer of TRIM55 B2 (dimer 1 in Supplemental Figure S2B), is consistent with the known composition of the dimeric TRIM fold. In dimer 1, E140s are located on the surface of the protein, whereas in the other TRIM55 B2 dimer (dimer 2) resulting from the crystallographic symmetry of TRIM63, the E140 residues contribute to the dimer interface (Supplemental Figure S2C).

The surface presentation of E140K variant clearly demonstrates the effect of replacing a negatively charged E140 with a positively charged lysine in the dimer interface. In the TRIM55 B2 dimer 2 (Fig. 1B), one of the E140s is involved in an extensive network of ionic

interactions and both of E140s interact with H164. In the E140K variant, these favorable interactions are lost (Fig. 1C). Interestingly, the analysis of the TRIM63 oligomeric structure revealed that in the presence of the B2 domain it formed higher-order oligomeric species but in the absence of B2 the protein was dimeric [17]. Thus, the dimer 2 interface where E140 resides is plausibly involved in forming higher-order oligomers of TRIM55. The structural comparison of the TRIM55 B2 model with the heterodimer of the RING domains of BRCA1 and BARD1 (PDB ID 1JM7) [18] (Supplemental Figure S2D) shows that E140 in the TRIM55 B2 monomer corresponds to the acidic D40 in BRCA1 facing towards the heterodimer interface in the BRCA1 - BARD1 complex. Similarly, E140 in the dimer 2 interface is likely to be involved in forming the heterodimeric complexes of TRIM55. As a conclusion, our results suggest that the formation of both higher-order oligomers and heterodimeric complexes might be disturbed in the TRIM55 E140K variant.

3.3 Loss of functional Trim55 in HL-1 cardiomyocytes alters gene expression regulation of contractility and cardiac stress

To study the functional effects of TRIM55 E140K variant, located in exon 3, *in vitro*, stable cardiomyocyte lines carrying *Trim55* variants were generated with CRISPR/Cas9 using mouse HL-1 cells as background. Out of 49 CRISPR-treated single-cell clones subjected to screening, two carried the E140K coding variant in their genome, both together with a deletion allele (E140K/- genotype) (Fig. 2A). One of these lines was randomly chosen for validations. No cell lines carrying homozygous E140K/E140K or heterozygous WT/E140K genotypes were identified among the generated clones. For comparison of the phenotype of the E140K/- line, predicted to be functionally a double-knockout, cell lines carrying heterozygote (WT/-) and homozygote (-/-) knockout genotypes were included in the analyses (Fig. 2A). The deletion alleles in all three variant lines caused a nonsense mutation, leading to a premature stop codon.

Lengths of protein products of deletion alleles were 158 amino acids in E140K/- line, 146 and 159 amino acids in -/- line and 146 amino acids in WT/- line.

Protein and mRNA expression levels in the cell lines were assessed with Western blotting and quantitative RT-PCR, respectively. In E140K/- line, the TRIM55 protein level was reduced approximately to 70% of the wildtype, the difference being borderline significant (P = 0.057; n = 4) (Fig. 2B). In -/- line, the protein expression was completely abolished, while in WT/- cells the expression was approximately 50% of the WT/WT line (P = 0.043; n = 4) (Fig. 2B). Similarly, *Trim55* mRNA expression was markedly reduced in -/- and WT/- lines, compared to WT/WT, even though the corrected P-values did not reach statistical significance level (Fig. 2C). In E140K/- cells, the mRNA expression level remained relatively unchanged as compared to WT/WT line (Fig. 2C). Binding sites of primers used in the RT-PCR analysis in exons 3 and 4 are shown in Supplemental Figure S3.

For systematic characterization of transcriptomic alterations caused by *Trim55* variants, the cell lines were subjected to whole-genome RNA sequencing to identify differentially expressed genes and signaling pathways implicated in heart failure. We performed unsupervised hierarchical clustering of the variant cell lines based on 82 most highly-regulated genes in the variant cell lines (selected based on their expression differences in the smallest 5% percentile of adjusted P-values, with a cut-off of $P < 7.06 \times 10^{-13}$, as compared to WT/WT cells), which grouped E140K/- and -/- lines together, and closer to WT/WT line, while WT/- samples formed their own cluster (Fig. 3A). No batch effects were observed between replicates within each cell line (Supplemental Figure S4).

Gene set enrichment analysis using gene ontology (GO) terms for differentially expressed genes in E140K/- line demonstrated enriched regulation of pathways related to muscle contraction, contractile structures, and heart and muscle development (adjusted P = 0.021; Fig. 3B), which are in line with the known functions of *Trim55*. When focusing on the

top-10 leading edge genes of the most regulated pathway in E140K/- cells (GO_REGULATION_OF_MUSCLE_CONTRACTION), the E140K/- and -/- samples clustered again together, underlining the deleterious effect of E140K as compared to WT/WT and WT/- samples, especially in *Nppa*, *Myl7* and *Adra2b* genes (Fig. 3C and 3D). These three top leading edge genes of the pathway were selected for validation by quantitative RT-PCR.

In the independent validation samples, expression level of *Nppa* was consistently higher in E140K/- cells ($P = 0.101$; n = 3), as compared to WT/WT samples, whereas *Nppa* expression was lower in WT/- samples ($P = 0.101$; n = 3) (Fig. 3D). Atrial natriuretic peptide encoded by *Nppa* is an established marker for cardiac stress and heart failure [19]. *Myl7* expression was also consistently lower in the E140K/- line ($P = 0.061$; n = 3), similarly to *Adra2b* ($P = 0.150$; n = 3) (Fig. 3D). We note that all the reported *P*-values are FDR-corrected, which together with small sample numbers explain the moderate significance levels. However, in the E140K/- line, the direction of regulation of all the validated genes were in concordance with the RNA sequencing results. These results indicate that the loss of functional *Trim55* regulates genes related to cardiac contractility and stress.

3.4 Trim55 E140K variant reduces cardiomyocyte viability and cell cycle progression and predisposes to hypertrophy

To investigate the phenotypic alterations in HL-1 cells carrying the defective *Trim55* variants, we measured functional readouts quantifying cellular viability, cell cycle progression and hypertrophy. It was observed that the viability of the cells was significantly reduced in the E140K/- cells as compared to the WT/WT cells ($P = 0.006$, n = 4) (Fig. 4A), as well as to WT/- cells ($P = 0.014$, n = 4), suggesting a damaging role of E140K variant.

To further evaluate the potential reason for the observed difference in the overall measure of viability or cell number, p21 expression as a marker for cell cycle progression was

assessed using Western analysis. In E140K/- cells, the p21 expression level was moderately higher as compared to WT/WT cells ($P = 0.093$; n = 5) (Fig. 4B). In RNA sequencing data, no differences in expression level of *CDKN1A*, which encodes p21, were detected in the variant cell lines, as compared to WT/WT (E140K/- vs WT/WT: fold change = 1.47, $P = 0.572$; -/- vs WT/WT: fold change = 1.17, $P = 0.999$; fold change = 1.21, $P = 0.793$). In flow cytometry-based cell cycle analysis using propidium iodide for DNA staining, E140K/- cells had significantly fewer cells in mitotic G2/M phase as compared to WT/WT cells ($P = 0.015$; n = 4) (Fig. 4C). As for WT/- cells, there were fewer cells in S phase as compared WT/WT cells ($P = 0.004$; n = 4), and accumulation of cells was observed in G2/M phase ($P = 0.015$, n = 4) (Fig. 4C), indicating either a more rapid progression of cell cycle or alternatively a stop of cell cycle progression at checkpoints other than for E140K/- cells. Although the viability of WT/- cells was not significantly higher as compared to WT/WT cells (Fig. 4A), the cells were observed to grow and become confluent faster than WT/WT cells in cell culture. Therefore, a cessation in cell cycle progression seems less likely.

For measuring the hypertrophic response, the cells were exposed to 48-hour treatment with 100 μM isoproterenol. In immunofluorescence analysis of the cell surface area with myosin heavy chain staining, each E140K/-, -/- and WT/- cell line demonstrated a significant increase in their normalized surface areas ($P = 0.001$, $P < 0.001$ and $P = 0.018$, respectively; n = 282-484 individual cells per each group), when challenged with isoproterenol, as compared to non-treated controls (Fig. 4D-E). In contrast, WT/WT cells did not show a hypertrophic response to isoproterenol treatment. For comparability, the data are normalized within each cell line separately (i.e., the median of non-treated controls is set to one), since the average cell sizes differed markedly between the cell lines (Supplemental Figure S5).

3.5 Trim55 E140K variant affects p62 and SRF protein levels, α-actinin expression and calcium transients in cardiomyocytes

To study the effects of *Trim55* variants on its E3 ubiquitin ligase activity, expression levels of the known *Trim55* interaction partners or ubiquitination targets SRF [9,20], p62 [21] and cardiac troponin I (cTnI) [22] were studied in the cell lines. P62 and SRF expression levels were lower in E140K/- cells compared to wildtype cells ($P = 0.004$ and $P = 0.034$, respectively, n = 3), and modestly lower in -/- cells compared to wildtype cells ($P = 0.061$ and $P = 0.072$, respectively, n = 3), while no changes were detected in cTnI expression (Supplemental Figure S6A-C). P62 expression was additionally lower in WT/- cells ($P = 0.002$). Ubiquitination of SRF or p62 was not detected after immunoprecipitation with protein-specific antibodies, followed by blotting with anti-poly- and mono-ubiquitin antibodies (Supplemental Figure S6D-E). Additionally, no changes were detected in total ubiquitination levels between the cell lines (Supplemental Figure S6F), which was expectable since TRIM55 is only one of multiple E3 ligases. Interestingly, lower expression levels of both p62 and SRF were detected in *Trim55* deficient cell lines although it may have been more expected to see their upregulation, assuming they are ubiquitination targets of TRIM55. This suggests a complex network of factors regulating the activity of these proteins.

To examine sarcomere structures in the variant cell lines, α-actinin stainings followed by immunofluorescence and confocal imaging were used. It was observed that α-actinin expression and organization was heterogeneous among cells within the cell lines. However, on average E140K/- cells, compared to WT/WT cells, demonstrated a higher staining intensity of α-actinin filaments ($P < 0.001$), which was analyzed using an automated algorithm to identify the myofibrillar structures (Supplemental Figure S7A-B). This reflects on the one hand higher expression of α-actinin in E140K/- cells (also observed in RNA-seq data, *ACTN2* expression fold-change = 3.89 compared to WT/WT cells, $P = 0.001$), and on the other hand aggregated

spots of α-actinin in these cells (Supplemental Figure S7A), which may indicate disorganization of myofibrils. In -/- and WT/- cells, the α-actinin filament staining was less intensive compared to WT/WT cells ($P < 0.001$ for both comparisons, Supplemental Figure S7A-B). Width-to-length ratio of filaments was also examined to reveal potential changes in filament morphology. While lengths and widths of filaments were greater in E140K/- cells and smaller in -/- and WT/- cells, compared to WT/WT cells (data not shown), the width-to-length ratios were virtually similar (median = 0.377 for WT/WT, 0.386 for E140K/-, 0.381 for -/- and 0.387 for WT/- cells), where the differences were statistically significant only for E140K/- ($P = 0.040$) and WT/- ($P = 0.007$), compared to WT/WT cells (Supplemental Figure S7C). TRIM55 E140K variant thus affects the expression and organization of α-actinin in sarcomeres.

Additionally, to study the excitability of the cells, we examined the calcium transients of the cells using Fluo-4 AM staining, both spontaneously and under pacing. No statistically significant differences in spontaneous frequencies or calcium transient amplitudes and decay times were detected (data not shown). The trend in frequencies was that TRIM55-variant cells demonstrated higher spontaneous frequencies (on average 0.15 Hz for E140K/-, 0.097 Hz for -/- and 0.11 Hz for WT/- cells), compared to WT/WT cells (on average 0.085 Hz). Representative traces of spontaneous transients are shown in Supplemental Figure S7D. However, when paced at the frequency of 0.5 Hz (Supplemental Figure S7E), E140K/- cells demonstrated significantly higher amplitude of calcium transients (Supplemental Figure S7F), with no differences in decay times (Supplemental Figure S7G). This higher excitability is potentially a multifactorial process, involving expression changes in both myofibrillar and calcium ion handling proteins. Interestingly, GO_CALCIUM_ION_BINDING pathway was one of the most highly-regulated pathways in E140K/- cells in RNA-seq analysis (Fig 2B). In pacing with 2 Hz frequency, all of the cell lines were capable to capture the rhythm (Supplemental Figure S7H, upper panels), even though they demonstrated also aberrant

rhythms (Supplemental Figure S7H, lower panels). Especially E140K/- cells repeatedly captured initially the pacing with 2:1 ratio, which was later decreased to 3:1 or less, as shown in the example trace (Supplemental Figure S7H, E140K/-, lower panel).

Taken together, E140K/- cells presented a markedly different phenotype than WT/WT or WT/- cells, supporting the damaging role of E140K variant. Interestingly, the numerical changes in cell viability and p21 expression were even more pronounced in E140K/- than in -/- cells, suggesting a possible dominant negative role for E140K variant. Moreover, overexpression of TRIM55 E140K in wildtype HL-1 cells reduced the cellular viability, as compared to TRIM55 WT-transfected cells ($P = 0.026$; n = 4) (Supplemental Figure S8A-B). However, no differences were observed in cell cycle progression (Supplemental Figure S8C). A significant hypertrophic response to isoproterenol was observed in control- and TRIM55 E140K-transfected cells, while there were no significant differences in TRIM55 WT-transfected cells (Supplemental Figure S8D-E). TRIM55 WT overexpression could thus protect from hypertrophy, in contrast to E140K variant. Furthermore, it is worth noting that cell sizes of untreated TRIM55 WT-transfected cells were greater than those of control- and E140K-transfected cells. These data demonstrate that E140K variant of TRIM55 might have negative effects on cardiomyocyte viability even when expressed in cells with wildtype protein.

3.6 Knockout of trim55a or overexpression of human TRIM55 E140K reduces cardiac contractility in zebrafish embryos

To further study the implications of TRIM55 E140K variant on the functionality of the heart *in vivo*, a zebrafish embryo model was used. First, the *trim55a* gene was knocked out from zebrafish embryos using transient CRISPR/Cas9 technique. The 1-4-cell stage embryos were injected with CRISPR constructs with a pool of three *trim55a* sgRNAs one day after fertilization and the phenotype was measured at four days after fertilization. A representative

sequencing chromatogram from the *trim55a* locus of an edited embryo harboring aberrant sequence after sgRNA binding sites is shown in Fig. 5A. On mRNA level, *trim55a* expression was significantly reduced (on average by 41%) after CRISPR treatment ($P < 0.001$, n = 5 batches of eight embryos pooled per treatment) (Supplemental Figure S9A). On protein level, a 55-kDa band detected in the Western blot analysis, corresponding to the predicted size of the known *trim55a* transcript, was on average 66% lower in *trim55a*-knockout embryos. The result was modestly significant ($P = 0.078$, n = 5 batches of eight embryos pooled per treatment), due to the high variability in control samples (Supplemental Figure S9B-C).

Videomicroscopically measured fractional shortening of the heart was significantly reduced in *trim55a*-targeting sgRNA-injected embryos, as compared to control sgRNA-injected embryos (median (IQR): 0.14 (0.10) vs. 0.17 (0.650); $P = 0.002$; n = 23 and 24, respectively) (Fig. 5B). There were no differences in the heart rate between any groups and no differences in fractional shortening between uninjected and control sgRNA-injected embryos (Fig. 5B). Additionally, to address possible off-target effects of *trim55a* sgRNAs, the three sgRNAs were injected also separately in an independent experiment. Reduction in fractional shortening was replicated in each sgRNA group (Supplemental Figure S10A). Heart rate was also higher in sgRNA #7- and #16-injected embryos compared to control sgRNA group (Supplemental Figure S10B). End-diastolic diameter was reduced by approximately 2–5% with *trim55a* knockdown by all sgRNAs, compared to control sgRNA group (Supplemental Figure S10C).

To specifically assess the effect of TRIM55 E140K, assuming its potential negative dominant role, the protein was expressed in constructs encoding TRIM55 WT and E140K with a heart specific cardiac myosin light chain 2 (*cmlc2*, *myl7*) promoter. A construct with the same backbone encoding GFP was used as the control. Heart-specific expression was confirmed with fluorescence microscopy (Fig. 5C). Fractional shortening was significantly lower in the embryos injected with either TRIM55 WT and E140K together as in heterozygous state or with

TRIM55 E140K construct alone, as compared to TRIM55 WT-injected embryos (median (IQR): 0.12 (0.033) for WT/E140K (n = 20) and 0.12 (0.045) for E140K alone (n = 16) vs. 0.16 (0.02) for WT alone (n = 25); $P = 0.004$ for both WT/E140K vs. WT and E140K vs. WT) (Fig. 5D). There were no observed differences in fractional shortening between control- and TRIM55 WT-injected embryos ($P = 0.236$; n = 27 and 25, respectively), neither between control-injected embryos and uninjected controls ($P = 0.142$, n = 27 and 18, respectively).

We observed no significant difference in heart rate between control-, TRIM55 WT- and WT/E140K-injected embryos, whereas heart rate was significantly increased by TRIM55 E140K injections, as compared to control-injected embryos (median (IQR): 118.5 (11.6) vs. 106.7 (7.5); P = 0.007; n = 16 and 27, respectively) or WT-injected ones (median (IQR): 118.5 (11.6) vs. 107.4 (9.5); $P = 0.007$; n = 16 and 25, respectively).

Finally, end-diastolic diameter (EDD) and end-systolic diameter (ESD) in CRISPR knockout experiment and TRIM55 overexpression experiment shown in Figure 5 were analyzed to address changes in the sizes of the ventricles. *Trim55a* CRISPR knockout slightly reduced EDD compared to uninjected and control-injected embryos while no differences in ESD were observed (Supplemental Figure S11A-B), similarly to the experiment with separate sgRNA injections (Supplemental Figure S10C). *Trim55a* knockout did not thus cause a dilated phenotype. TRIM55 overexpression did not affect ventricular size (Supplemental Figure S11C-D).

These data indicate that the overexpression of TRIM55 E140K, but not TRIM55 WT, affects the functionality of the heart. This further supports the damaging and dominant-negative role of the E140K variant.

4. Discussion

To improve our understanding of the genetic background of heart failure risk, we screened for novel heart failure-associated genetic variants in the Finnish population and selected a missense variant in *TRIM55* for functional validations *in vitro* and *in vivo*. This variant, rs138811034, encoding E140K variant in the protein, was shown to be functionally deficient, demonstrating even dominantly negative effects. Although *TRIM55* has earlier been shown to have implications on heart failure [7,11,12], the details of cellular level perturbations caused by any *TRIM55* variant have not been characterized earlier. We therefore carried out a systematic functional analysis of the E140K variant using CRISPR/Cas9 gene editing in mouse cardiomyocytes and zebrafish embryos.

In our screening for heart failure-associated variants, moderately significant associations for variants in the known heart failure loci were observed, including *ACE* [6], *ANKRD1*, *DSG2*, *MYBPC3* and *TTN* [5]. We note that the variants identified in our statistical analysis were not the heart failure-associated functional variants identified in these genes in the previous studies. This is potentially due to lack of power, resolution of the genotyping array or population-specific factors. However, we did not study the possible linkage between the known variants and the ones identified in our analysis. The lead SNP in chromosome 8 was located in the *ADHFE1* gene that is involved in adipogenesis [23], and it has also been shown to have oncogenic functions [24]. In the search for variants in high LD with this lead SNP, we initially identified an intronic variant in *DNAJC5B* (rs112144279, $r^2 = 0.64$) (Table 2). Interestingly, another variant in *DNAJC5B* has been shown to be associated with the effectiveness of pravastatin therapy to prevent coronary artery disease events [25]. The *DNAJC5B* variant was, however, omitted from the functional analyses due to residing in an intron.

The rs138811034 variant in *TRIM55* that was chosen for functional validations is the third most frequent missense variant of *TRIM55* in the ExAC database [14,26]. Rare

nonsynonymous (i.e. missense, insertion or deletion) variants in *TRIM55,* and also in *TRIM63,* have been shown to contribute to more severe phenotype of human hypertrophic cardiomyopathy [16]. The patients with pathogenic variants in these genes were younger and had greater left ventricular wall thickness than patients without these variants [16]. However, the E140K variant was not identified in this cohort.

In our results on HL-1 cardiomyocytes, CRISPR-mediated knockout of *Trim55* was sufficient to cause a significant hypertrophic response to isoproterenol and it also affected the cell cycle progression. However, cell cycle was not among the significantly regulated pathways in the GSEA analysis, and for instance, no alterations in *CDKN1A* expression were detected in RNA sequencing. This indicates that *TRIM55* deletion potentially affects the cell cycle at post-transcriptional or post-translational level. In RNA-seq validation results, *Nppa* mRNA expression level was higher in E140K/- and -/- cells while it was lower in WT/- cells compared to WT/WT cells. It is likely that the observed difference is affected by the SRF-regulated *Nppa* expression, as we observed in Western blot analyses the relative upregulation of a shorter, possibly inhibitory isoform of SRF studied by Davis et al. [27] in WT/- cells (Supplemental Figure S6A-D). Moreover, it has been shown that complete *SRF* knockout in mice causes cardiomyopathy and increases *Nppa* expression [28,29]**.** We further confirmed the role of *Trim55* in cardiomyocyte phenotype with siRNA-mediated knockdown of *Trim55* expression in WT HL-1 cells, which reduced the cellular viability (Supplemental Figure S12A-B), and hence provides complementary support for the phenotypic effect. In zebrafish embryos, the knockout of *trim55a* alone was sufficient to decrease cardiac contractility *in vivo*. Our results, combined with the previous studies, therefore suggests that functionality of TRIM55 modulates the susceptibility to and the phenotype of heart failure, but many of its variants, including E140K, have so far remained uncharacterized.

In our functional experiments, *Trim55* E140K/- cells were significantly less viable than WT/WT and WT/- cells and numerically less viable than -/- cells. On the other hand, overexpression of human TRIM55 E140K reduced the viability of cardiomyocytes as compared to TRIM55 WT overexpression. Cardiomyocytes transfected with TRIM55 E140K demonstrated a significant hypertrophic response to isoproterenol while TRIM55 WT-transfected cells did not. Similarly in zebrafish embryos, overexpression of human TRIM55 E140K, both alone and together with TRIM55 WT, impaired cardiac contractility while TRIM55 WT alone did not. At the same time, heart rate was increased by TRIM55 E140K overexpression, as compared to TRIM55 WT. Additionally, differences in heart rate were observed in *trim55a* CRISPR experiments between control injected and sgRNA#7- and #16-injected embryos. These changes reflect potentially compensatory responses to maintain cardiac output. Heart dimensions were not larger in embryos with *trim55a* knockout or TRIM55 E140K overexpression, likely due to robust functional reserve. Finally, it is worth noting, that in E140K/- cells the calcium transient amplitude was higher, compared to WT/WT cells. This suggests that the observed lower contractility in the zebrafish carrying TRIM55 variants is not due to impaired calcium cycling. Taken together, E140K seems to have effects on cardiac functions even when expressed together with endogenous TRIM55 WT, which suggests a dominant negative role.

One possible mechanistic explanation for the negative impact is that expressed TRIM55 E140K could impact the subcellular localization of the transcription factor serum response factor (SRF) in different manner than the wildtype protein. TRIM55 has been shown to reduce the amount of SRF in the nucleus [20]. In our GSEA results for motif gene sets, which consist of gene sets with genes grouped according to their transcriptional regulatory elements, multiple SRF-related gene sets were among the most significantly regulated ones in E140K/- cells, as well as in -/- and WT/- cells (Supplemental Table 1). Thus, the SRF-related signaling

alterations are not unique to E140K cells only. However, our results suggest that the effect of E140K is potentially more harmful than that of simple deletion of the gene. If it indeed is a negative dominant variant, E140K could be detrimental even in its heterozygous form. This should be further assessed in heterozygous WT/E140K models preclinically or in larger human cohorts *in vivo*.

As TRIM55 E140K variant potentially increases the susceptibility of heart failure, it could be used as a prognostic marker in the clinical genetic screening for heart failure patients. Targeting TRIM55 pharmacologically may not be a feasible approach for drug treatment of heart failure, as the protein seems to be necessary for normal cardiac function. On the other hand, the other members of the pathways TRIM55 is involved in, such as SRF signaling pathway, might be viable alternatives as for therapeutic targeting. SRF is a potent inducer of hypertrophy [30]. Interestingly, an inhibitor of SRF has been developed for the treatment of fibrosis [31]. Testing this molecule in cardiac hypertrophy or heart failure models is an exciting avenue for further research.

A particular limitation of this study is the relatively small number of cases included in the genetic association study. We identified signals from a few established heart failure-associated loci, but without reaching genome-wide-level of significance. However, as our aim was to find novel genetic markers and test their functional implications *in vitro* and *in vivo*, the results are not based solely on GWAS findings. The TRIM55 E140K variant was tested on HL-1 cardiomyocytes, which provide a robust but not the most sophisticated cardiomyocyte model. These cells were selected since they are easy to maintain and they can be passaged multiple times, as opposed to primary neonatal cardiomyocytes. Testing the variant in pluripotent human stem cell-derived cardiomyocytes would bring the approach to a human cell model, which is an important direction for future studies. RNA sequencing experiment was performed on only two biological replicates per cell line. However, no batch effects were detected between the

replicates, and RT-PCR validation results of the leading edge genes were concordant to RNA sequencing results. The *in vivo* experiments in zebrafish embryo models were performed less than five days after fertilization. Therefore, the findings at that time point might be embryo-specific and the phenotype could be reversed at a later stage of development. Our results warrant assessing the implications of the variant in an adult model, preferably mammalian. We note, however, that this is the first in-detail assessment of a *TRIM55* coding variant in heart failure, demonstrating how genetic association studies could be enhanced by functional validations *in vitro* and *in vivo*.

In conclusion, the TRIM55 E140K variant was shown to be damaging and potentially dominantly negative, and it has functional implications on several cardiomyocyte functions. TRIM55 E140K is a potential genetic marker for heart failure prognosis or pathogenesis, which warrants further studies to confirm its significance in the human heart.

Acknowledgements

The authors thank Sanna Timonen, Nora Linnavirta and Daria Bulanova at FIMM and the Core facilities Sequencing Unit and Bioinformatics Unit at FIMM Technology Centre supported by University of Helsinki and Biocenter Finland for excellent technical and methodological assistance. Dr. Antti Hassinen and the High Content Imaging and Analysis (HCA) unit at the Institute for Molecular Medicine Finland (FIMM), HiLIFE, University of Helsinki, and Biocenter Finland are acknowledged for high content microscopy imaging and image analysis. We also thank the bioinformatics (J.V. Lehtonen), translational activities and structural biology infrastructure support from Biocenter Finland and Instruct-FI, and CSC IT Center for Science for computational infrastructure support at the Structural Bioinformatics Laboratory, Åbo Akademi University. The FINRISK data used for the research were obtained from THL Biobank. We thank all participants for their generous contribution in the FINRISK study. The

flow cytometry analysis was performed at the HiLife Flow Cytometry Unit, University of Helsinki and zebrafish experiments at the Zebrafish Core and Cell Imaging Core (both Turku Bioscience Centre, University of Turku and Åbo Akademi University).

Funding

This work has been funded by grants from The Finnish Cultural Foundation (Varsinais-Suomi Regional Fund), University of Turku, The Paulo foundation, Inkeri ja Mauri Vänskän säätiö, Orion Research Foundation sr, Academy of Finland, Cancer Society of Finland, Sigrid Juselius Foundation and Tor, Joe and Pentti Borg's Foundation.

Disclosures

JH is employed by and has ownership interest in Abomics Ltd. KE has ownership interest in Abomics Ltd., Orion Ltd. and Roche.

References

[1] A. Mosterd, A.W. Hoes, Clinical epidemiology of heart failure, Heart. 93 (2007) 1137–1146. https://doi.org/10.1136/hrt.2003.025270.

[2] G.S. Bleumink, A.M. Knetsch, M.C.J.M. Sturkenboom, S.M.J.M. Straus, A. Hofman, J.W. Deckers, et al., Quantifying the heart failure epidemic: Prevalence, incidence rate, lifetime risk and prognosis of heart failure - The Rotterdam Study, Eur. Heart J. 25 (2004) 1614–1619. https://doi.org/10.1016/j.ehj.2004.06.038.

[3] D.S. Lee, M.J. Pencina, E.J. Benjamin, T.J. Wang, D. Levy, C.J. O'Donnell, et al., Association of parental heart failure with risk of heart failure in offspring., N. Engl. J. Med. 355 (2006) 138–47. https://doi.org/10.1056/NEJMoa052948.

[4] U. Tayal, S. Prasad, S.A. Cook, Genetics and genomics of dilated cardiomyopathy and

systolic heart failure, Genome Med. 9 (2017) 20. https://doi.org/10.1186/s13073-017-0410-8.

[5] T.J. Cahill, H. Ashrafian, H. Watkins, Genetic cardiomyopathies causing heart failure, Circ. Res. 113 (2013) 660–675. https://doi.org/10.1161/CIRCRESAHA.113.300282.

[6] M. Guo, G. Guo, X. Ji, Genetic polymorphisms associated with heart failure: A literature review, J. Int. Med. Res. 44 (2016) 15–29. https://doi.org/10.1177/0300060515604755.

[7] S. Perera, M.R. Holt, B.S. Mankoo, M. Gautel, Developmental regulation of MURF ubiquitin ligases and autophagy proteins nbr1, p62/SQSTM1 and LC3 during cardiac myofibril assembly and turnover, Dev. Biol. 351 (2011) 46–61. https://doi.org/10.1016/j.ydbio.2010.12.024.

[8] M.S. Willis, K.M. Wadosky, J.E. Rodríguez, J.C. Schisler, P. Lockyer, E.G. Hilliard, et al., Muscle ring finger 1 and muscle ring finger 2 are necessary but functionally redundant during developmental cardiac growth and regulate E2F1-mediated gene expression in vivo, Cell Biochem. Funct. 32 (2014) 39–50. https://doi.org/10.1002/cbf.2969.

[9] C.C. Witt, S.H. Witt, S. Lerche, D. Labeit, W. Back, S. Labeit, Cooperative control of striated muscle mass and metabolism by MuRF1 and MuRF2, EMBO J. 27 (2008) 350–360. https://doi.org/10.1038/sj.emboj.7601952.

[10] M.S. Willis, C. Ike, L. Li, D.Z. Wang, D.J. Glass, C. Patterson, Muscle ring finger 1, but not muscle ring finger 2, regulates cardiac hypertrophy in vivo, Circ. Res. 100 (2007) 456–459. https://doi.org/10.1161/01.RES.0000259559.48597.32.

[11] J. He, M.T. Quintana, J. Sullivan, T. Parry, T. Grevengoed, J.C. Schisler, et al., MuRF2 regulates PPARγ1 activity to protect against diabetic cardiomyopathy and enhance weight gain induced by a high fat diet, Cardiovasc. Diabetol. 14 (2015) 1–24.

https://doi.org/10.1186/s12933-015-0252-x.

[12] P.R. Prestes, F.Z. Marques, G. Lopez-Campos, S.A. Booth, M. McGlynn, P. Lewandowski, et al., Tripartite motif-containing 55 identified as functional candidate for spontaneous cardiac hypertrophy in the rat locus cardiac mass 22, J. Hypertens. 34 (2016) 950–958. https://doi.org/10.1097/HJH.0000000000000875.

[13] K. Borodulin, E. Vartiainen, M. Peltonen, P. Jousilahti, A. Juolevi, T. Laatikainen, et al., Forty-year trends in cardiovascular risk factors in Finland, Eur. J. Public Health. 25 (2015) 539–546. https://doi.org/10.1093/eurpub/cku174.

[14] M. Lek, K.J. Karczewski, E. V Minikel, K.E. Samocha, E. Banks, T. Fennell, et al., Analysis of protein-coding genetic variation in 60,706 humans, Nature. 536 (2016) 285–91. https://doi.org/10.1038/nature19057.

[15] W. McLaren, L. Gil, S.E. Hunt, H.S. Riat, G.R.S. Ritchie, A. Thormann, et al., The Ensembl Variant Effect Predictor, Genome Biol. 17 (2016) 122. https://doi.org/10.1186/s13059-016-0974-4.

[16] M. Su, J. Wang, L. Kang, Y. Wang, Y. Zou, X. Feng, et al., Rare variants in genes encoding MuRF1 and MuRF2 are modifiers of hypertrophic cardiomyopathy, Int. J. Mol. Sci. 15 (2014) 9302–9313. https://doi.org/10.3390/ijms15069302.

[17] M. Mrosek, S. Meier, Z. Ucurum-Fotiadis, E. von Castelmur, E. Hedbom, A. Lustig, et al., Structural analysis of B-Box 2 from MuRF1: Identification of a novel self-association pattern in a RING-like fold, Biochemistry. 47 (2008) 10722–10730. https://doi.org/10.1021/bi800733z.

[18] P.S. Brzovic, P. Rajagopal, D.W. Hoyt, M. King, R.E. Klevit, Structure of a BRCA1 – BARD1 heterodimeric RING – RING, Nat. Struct. Biol. 8 (2001) 833–7.

[19] W. Song, H. Wang, Q. Wu, Atrial natriuretic peptide in cardiovascular biology and disease (NPPA), Gene. 569 (2015) 1–6. https://doi.org/10.1016/j.gene.2015.06.029.

[20] S. Lange, F. Xiang, A. Yakovenko, A. Vihola, P. Hackman, E. Rostkova, et al., The kinase domain of titin controls muscle gene expression and protein turnover, Science (80-.). 308 (2005) 1599–1603. https://doi.org/10.1126/science.1110463.

[21] V. Pizon, S. Rybina, F. Gerbal, F. Delort, P. Vicart, G. Baldacci, et al., MURF2B, a Novel LC3-Binding Protein, Participates with MURF2A in the Switch between Autophagy and Ubiquitin Proteasome System during Differentiation of C2C12 Muscle Cells, PLoS One. 8 (2013) 1–21. https://doi.org/10.1371/journal.pone.0076140.

[22] S.H. Witt, H. Granzier, C.C. Witt, S. Labeit, MURF-1 and MURF-2 Target a Specific Subset of Myofibrillar Proteins Redundantly: Towards Understanding MURF-dependent Muscle Ubiquitination, J. Mol. Biol. 350 (2005) 713–722. https://doi.org/10.1016/j.jmb.2005.05.021.

[23] J.Y. Kim, K.S. Tillison, S. Zhou, J.H. Lee, C.M. Smas, Differentiation-Dependent Expression of Adhfe1 in Adipogenesis, Arch Biochem Biophys. 464 (2007) 100–111.

[24] P. Mishra, W. Tang, S. Ambs, ADHFE1 is a MYC-linked oncogene that induces metabolic reprogramming and cellular de-differentiation in breast cancer, Mol. Cell. Oncol. 5 (2018) e1432260. https://doi.org/10.1080/23723556.2018.1432260.

[25] D. Shiffman, S. Trompet, J.Z. Louie, C.M. Rowland, J.J. Catanese, O.A. Iakoubova, et al., Genome-wide study of gene variants associated with differential cardiovascular event reduction by pravastatin therapy, PLoS One. 7 (2012) e38240. https://doi.org/10.1371/journal.pone.0038240.

[26] Exome Aggregation Consortium. ExAC Browser., (2019). http://exac.broadinstitute.org (accessed June 4, 2019).

[27] F.J. Davis, M. Gupta, S.M. Pogwizd, E. Bacha, V. Jeevanandam, M.P. Gupta, Increased expression of alternatively spliced dominant-negative isoform of SRF in human failing hearts, Am. J. Physiol. - Hear. Circ. Physiol. 282 (2002) H1521-1533.

https://doi.org/10.1152/ajpheart.00844.2001.

[28] A. Parlakian, C. Charvet, B. Escoubet, M. Mericskay, J.D. Molkentin, G. Gary-Bobo, et al., Temporally controlled onset of dilated cardiomyopathy through disruption of the SRF gene in adult heart, Circulation. 112 (2005) 2930–2939. https://doi.org/10.1161/CIRCULATIONAHA.105.533778.

[29] Y. Guo, B.D. Jardin, P. Zhou, I. Sethi, B.N. Akerberg, C.N. Toepfer, et al., Hierarchical and stage-specific regulation of murine cardiomyocyte maturation by serum response factor, Nat. Commun. (2018). https://doi.org/10.1038/s41467-018-06347-2.

[30] N. Frey, E.N. Olson, Cardiac Hypertrophy: The Good, the Bad, and the Ugly, Annu. Rev. Physiol. 65 (2003) 45–79. https://doi.org/10.1146/annurev.physiol.65.092101.142243.

[31] C. Yu-Wai-Man, B. Spencer-Dene, R.M.H. Lee, K. Hutchings, E.M. Lisabeth, R. Treisman, et al., Local delivery of novel MRTF/SRF inhibitors prevents scar tissue formation in a preclinical model of fibrosis, Sci. Rep. 7 (2017) 518. https://doi.org/10.1038/s41598-017-00212-w.

Figure legends

Figure 1. Missense E140K variant in TRIM55 is in high LD with a variant highly associated with heart failure.

A) A LocusZoom plot of rs117667921 in chromosome 8 associated with heart failure. The exonic variant rs138811034, encoding E140K protein variant, in *TRIM55* (highlighted in red square) was found out to be in high LD (D' = 1) with the lead variant rs117667921. Rs138811034 is not depicted in the figure since its independent association with heart failure was not statistically significant (P = 0.377) and its P-value was below the threshold for the variants shown here. B) The effect on E140K variation on the surface charge of TRIM55 B2. E140 is located on the dimer 2 interface and contributes to the negatively charged surface area in the wild-type protein. One of the monomers of dimer 2 is shown as surface and the other one as orange cartoon. The zinc ions are shown as spheres. C) K140 in the E140K variant switches the surface area positively charged, which plausibly has a harmful effect on the formation of higher-order oligomers and heterodimeric interactions.

Figure 2. Characterization of HL-1 cardiomyocyte-derived cell lines carrying Trim55 variants.

A) Sequencing chromatograms of *Trim55* of the cell lines used in validations. Underlined part in the sequence of WT/WT cell line depicts the binding site of the antisense sgRNA used in generating the mutant lines (PAM motif underlined in red). In E140K/- line, the E140K-coding variant (c.418G>A) is shown boxed and marked with an asterisk. Additionally, three silent mutations included in the HDR template to prevent further binding of sgRNA after editing are shown boxed in the same allele. Corresponding wildtype sequences after short deletions in deletion alleles are shown boxed. Corresponding protein sequences, with amino acids differing from wildtype marked in red, are shown under the sequences. B) A representative Western blot image and quantitation of TRIM55 protein expression from four independent samples of

Trim55 variant cell lines. Molecular weight scales next to Western blot images are in kilodaltons. C) *Trim55* mRNA expression analysis with quantitative RT-PCR from three independent samples of *Trim55* variant cell lines.

Figure 3. Genes related to cardiac contractility and stress are regulated in Trim55 E140K/- cells.

A) Unsupervised hierarchical clustering of *Trim55* variant cell lines according to 82 most highly regulated genes in all variant cell lines. WT/- cells form a distinct cluster while E140K/- and -/- cells cluster together. B) The most significantly regulated GO term gene sets in E140K/- cells as compared to WT/WT cells in GSEA analysis. NES, normalized enrichment score. C) Heatmap representation of unsupervised hierarchical clustering of *Trim55* variant cell lines according to top-10 leading edge genes of GO_REGULATION_OF_MUSCLE_CONTRACTION pathway. E140K/- and -/- cells cluster together as opposed to the cluster of WT/WT and WT/- cells. D) Quantitative RT-PCR validation of the three leading edge genes in the pathway from three independent validation samples. In E140K/- cells, the expression of *Nppa*, *Myl7* and *Adra2b* mRNA (normalized to *B2m* expression) was in concordance with RNA-seq results as compared to WT/WT cells. Bars represent means and error bars SEMs (n = 3 for RT-PCR experiments and n = 2 for RNA-seq). Results for each gene were normalized to control gene *B2m* and the expression level of WT/WT was set to one.

Figure 4. Trim55 E140K/- cells demonstrate reduced viability and decreased cell cycle progression and are prone to hypertrophy.

A) Cellular viability measured with CTG assay from *Trim55* variant cell lines grown on 96-well plate wells (n = 3 for all cell lines). B) A representative Western blot image and

quantitation of p21 protein expression from five independent samples of *Trim55* variant cell lines. C) Flow cytometry-based cell cycle analysis of *Trim55* variant cell lines after PI staining (n = 4 for all cell lines). Molecular weight scales next to Western blot images are in kilodaltons. D) Representative immunofluorescence images of *Trim55* variant cell lines treated with or without 100 μM of isoproterenol (ISO) for 48 hours to induce hypertrophy. Cells were stained with anti-myosin heavy chain antibody (green) to visualize cell surface area and nuclei were visualized with Hoechst (blue). Scale bar, 50 μm. E) Boxplot presentation of quantitated cell surfaces from *Trim55* variant cell lines from isoproterenol experiment. Cell surfaces were manually traced from immunofluorescence images. Due to variation in average cell sizes in different cell lines, medians of untreated controls of all cell lines are normalized to unity for visualization purposes (282-484 cells per each group were analyzed).

Figure 5. CRISPR-mediated knockout of trim55a or overexpression of human TRIM55 E140K reduce cardiac contractility in zebrafish embryos.

A) A representative sequencing chromatogram from a *trim55a*-edited zebrafish embryo around the sgRNA binding sites in exon 2. The binding site of *trim55a* sgRNAs are shown underlined (PAM motif underlined with red). The double peaks are caused by disruption of the genome. B) Boxplot presentations of fractional shortening and heart rate (beats per minute) measured at four days post fertilization from uninjected embryos (n = 16) and embryos injected at 1-4-cell stage with control sgRNAs (n = 24) or *trim55a*-targeting sgRNAs (n = 23). C) Representative brightfield and fluorescence images of a GFP control plasmid-injected embryo demonstrating heart- specific expression of the construct (boxed). Scale bar, 500 μm. D) Boxplot presentations of fractional shortening and heart rate (beats per minute) measured at four days post fertilization from uninjected embryos (n = 18) and embryos injected at 1-4-cell stage with GFP-control plasmid (n = 27), human TRIM55 WT plasmid (n

= 25), both TRIM55 WT and E140K plasmid (n = 20) or TRIM55 E140K plasmid alone (n = 16).

Figures

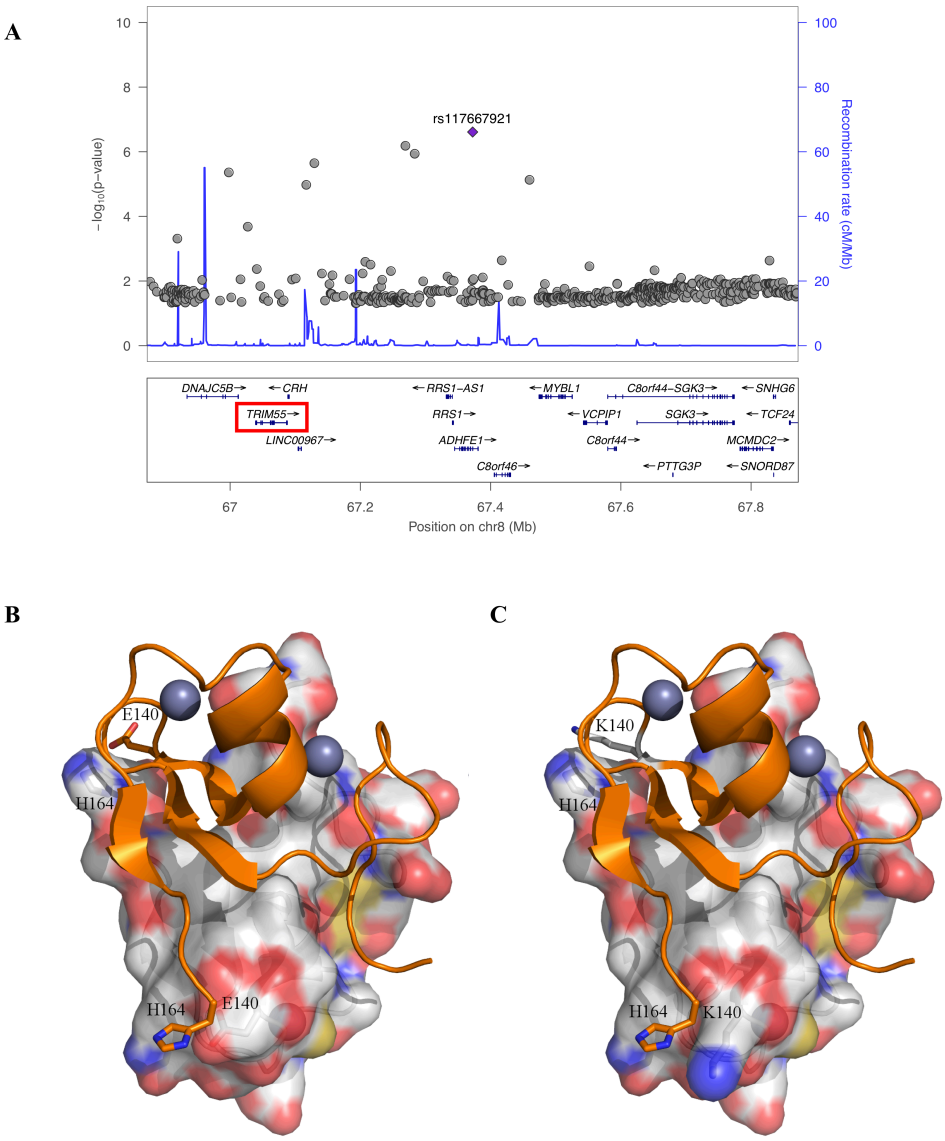

Fig. 1

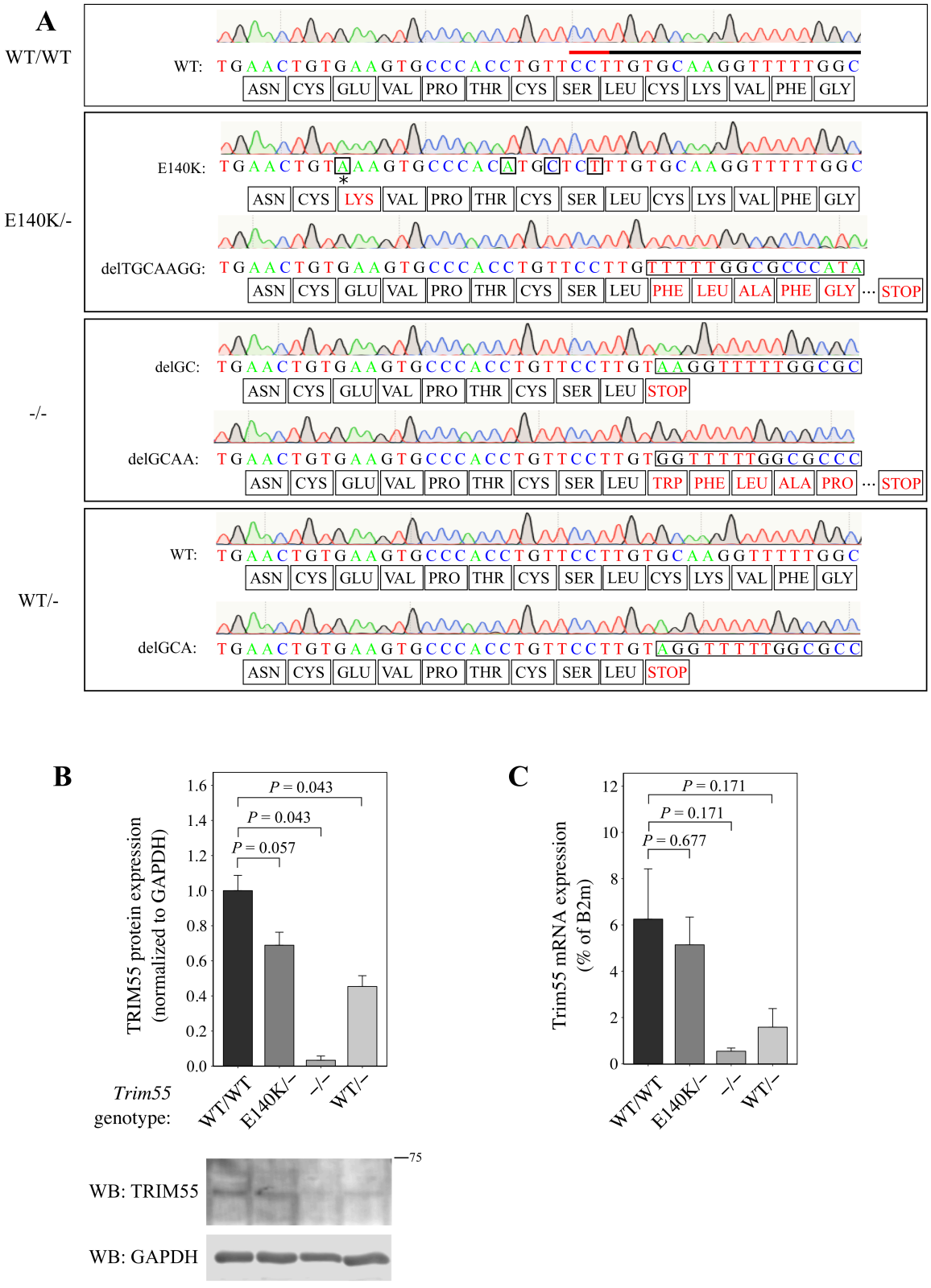
A
WT/WT
WT:
ASN CYS GLU VAL PRO THR CYS SER LEU CYS LYS VAL PHE GLY
E140K/-
E140K:
ASN CYS LYS VAL PRO THR CYS SER LEU CYS LYS VAL PHE GLY
delTGCAAGG:
ASN CYS GLU VAL PRO THR CYS SER LEU PHE LEU ALA PHE GLY ··· STOP
-/-
delGC:
ASN CYS GLU VAL PRO THR CYS SER LEU STOP
delGCAA:
ASN CYS GLU VAL PRO THR CYS SER LEU TRP PHE LEU ALA PRO ··· STOP
WT/-
WT:
ASN CYS GLU VAL PRO THR CYS SER LEU CYS LYS VAL PHE GLY
delGCA:
ASN CYS GLU VAL PRO THR CYS SER LEU STOP
B
TRIM55 protein expression (normalized to GAPDH)
P = 0.043
P = 0.043
P = 0.057
Trim55 genotype:
WT/WT
E140K/–
–/–
WT/–
WB: TRIM55
75
WB: GAPDH
C
Trim55 mRNA expression (% of B2m)
P = 0.171
P = 0.171
P = 0.677
WT/WT
E140K/–
–/–
WT/–

Fig. 2

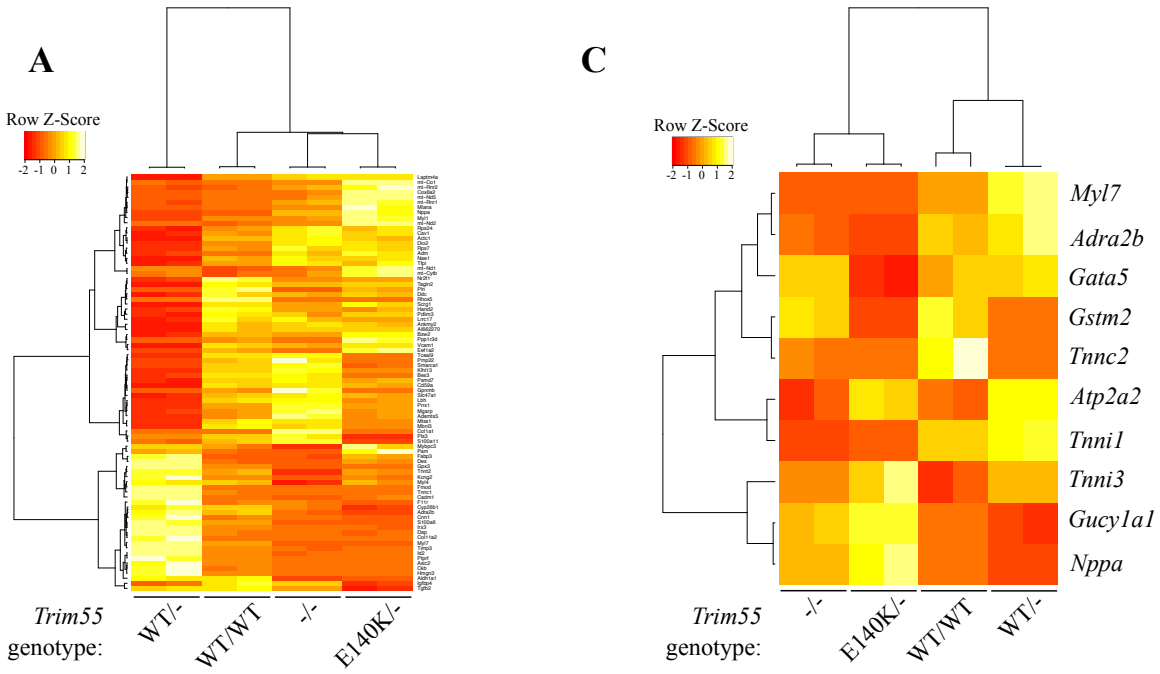

B

Pathway	Adj. *P*-value	NES	Pathway size
GO_REGULATION_OF_MUSCLE_CONTRACTION	0.021	1.510	142
GO_MUSCLE_SYSTEM_PROCESS	0.021	1.479	259
GO_REGULATION_OF_MUSCLE_SYSTEM_PROCESS	0.021	1.458	194
GO_EXTRACELLULAR_STRUCTURE_ORGANIZATION	0.021	1.444	192
GO_MUSCLE_CONTRACTION	0.021	1.442	211
GO_CONTRACTILE_FIBER	0.021	1.428	219
GO_REGULATION_OF_HEART_CONTRACTION	0.021	1.418	202
GO_GENERATION_OF_PRECURSOR_METABOLITES_AND_ENERGY	0.021	1.413	265
GO_MUSCLE_TISSUE_DEVELOPMENT	0.021	1.398	288
GO_CALCIUM_ION_BINDING	0.021	1.389	363
GO_CIRCULATORY_SYSTEM_PROCESS	0.021	1.386	294
GO_REGULATION_OF_SYSTEM_PROCESS	0.021	1.386	385
GO_WOUND_HEALING	0.021	1.353	368
GO_RESPONSE_TO_WOUNDING	0.021	1.344	440
GO_PURINE_CONTAINING_COMPOUND_METABOLIC_PROCESS	0.021	1.336	319
GO_ACTIN_CYTOSKELETON	0.021	1.335	436
GO_MUSCLE_STRUCTURE_DEVELOPMENT	0.021	1.322	425
GO_SKELETAL_SYSTEM_DEVELOPMENT	0.021	1.318	363
GO_HEART_DEVELOPMENT	0.021	1.307	490

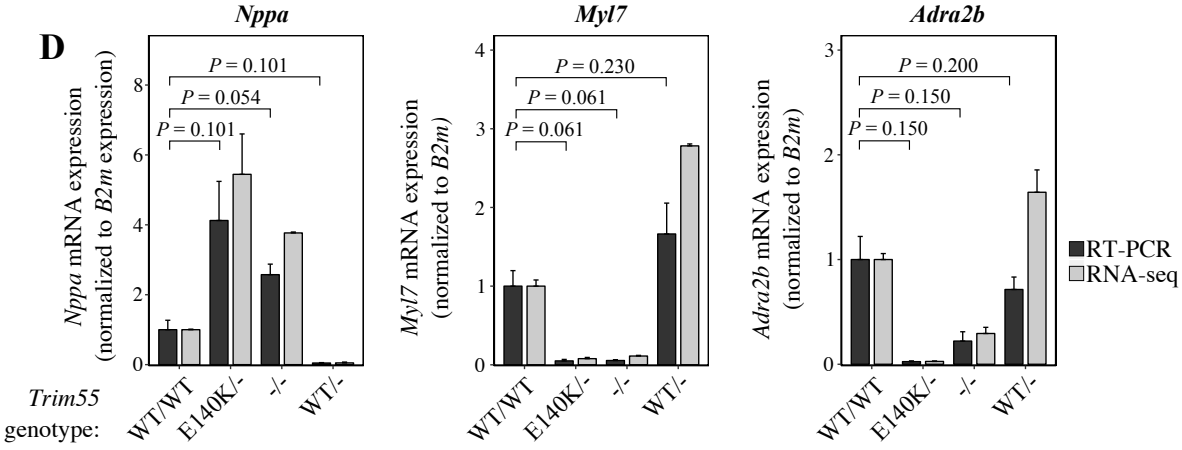

Fig. 3

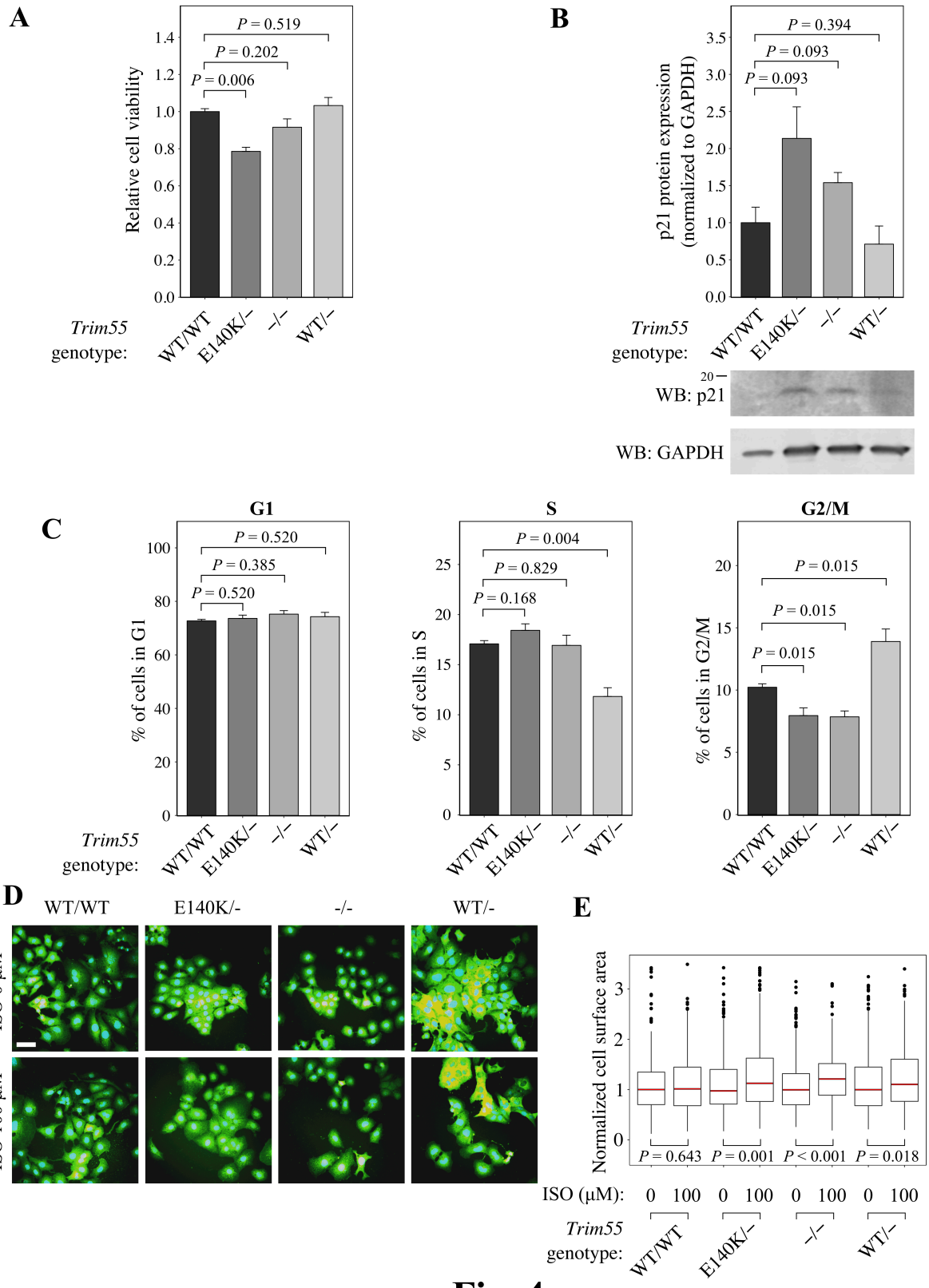
A
Relative cell viability
P = 0.519
P = 0.202
P = 0.006
Trim55 genotype:
WT/WT
E140K/–
–/–
WT/–
B
p21 protein expression (normalized to GAPDH)
P = 0.394
P = 0.093
P = 0.093
WB: p21
WB: GAPDH
C
G1
S
G2/M
% of cells in G1
% of cells in S
% of cells in G2/M
P = 0.520
P = 0.385
P = 0.520
P = 0.004
P = 0.829
P = 0.168
P = 0.015
P = 0.015
P = 0.015
D
WT/WT
E140K/-
-/-
WT/-
ISO 0 µM
ISO 100 µM
E
Normalized cell surface area
P = 0.643
P = 0.001
P < 0.001
P = 0.018
ISO (µM): 0 100 0 100 0 100 0 100
Trim55 genotype:
WT/WT
E140K/–
–/–
WT/–

Fig. 4

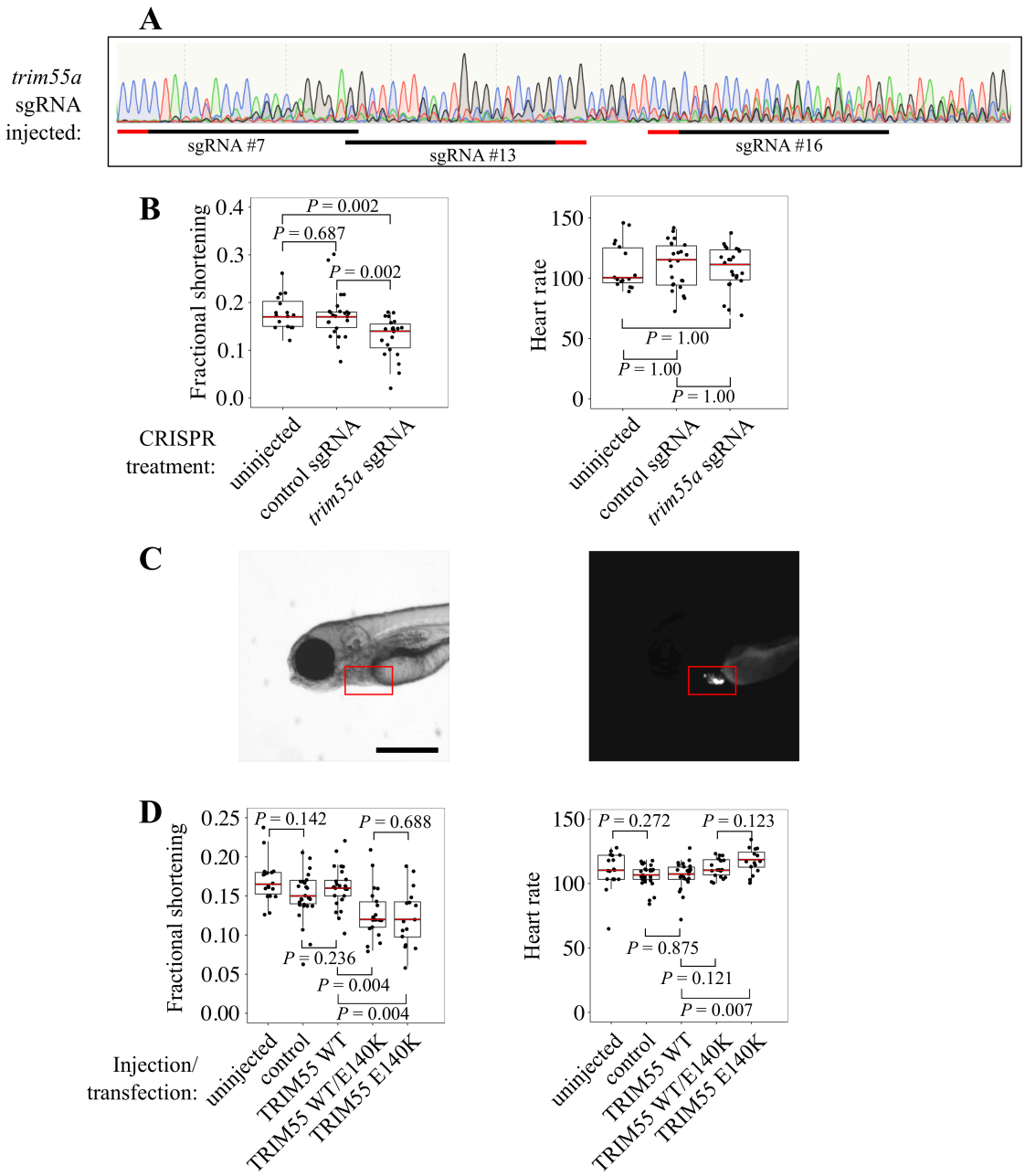
A
trim55a sgRNA injected:
sgRNA #7
sgRNA #13
sgRNA #16
B
Fractional shortening
P = 0.002
P = 0.687
P = 0.002
Heart rate
P = 1.00
P = 1.00
P = 1.00
CRISPR treatment:
uninjected
control sgRNA
trim55a sgRNA
C
D
Fractional shortening
P = 0.142
P = 0.688
P = 0.236
P = 0.004
P = 0.004
Heart rate
P = 0.272
P = 0.123
P = 0.875
P = 0.121
P = 0.007
Injection/ transfection:
uninjected
control
TRIM55 WT
TRIM55 WT/E140K
TRIM55 E140K

Fig. 5